Construction of hollow urchin-like carbon frameworks with Co, P, N doping and encapsulated Co/Co_2P heterojunction as bifunctional electrocatalysts for Zn-air batteries

Experimental section

Synthesis of polystyrene (PS) spheres: PS spheres were prepared by a previously reported method [1]. Typically, 20 mL of styrene and 20 mL of NaOH solution (1 mol L^{-1}) were added into a separatory funnel. After adequate oscillation, the solution was left to rest for about 10 min until significant stratification was observed. The above process was repeated twice to obtain an initiator-free styrene. Then, the purified styrene, acrylic acid (0.4 g) and deionized water (150 mL) were added into a three-neck flask, and the mixture was stirred at 70 °C under N_2 atmosphere. Afterword, 10 mL of ammonium persulfate (APS, 0.1 mol L^{-1}) was added and stirred for 24 h. Therewith, PS spheres were obtained after centrifugal separation, washing and drying at 80 °C in vacuum oven.

***Synthesis of HCoPNC*:** The as-prepared PS@PDA-Co was heated to 600 °C at a rate of 5 °C min^{-1} and kept for 2 h under N_2 atmosphere. After cooling to room temperature, the powder was collected (denoted as HCoNC). Then, 10 mg of the above powder and 200 mg of NaH_2PO_2 were placed at the downstream and upstream of tube furnace at N_2 flow, respectively. Then, the tube furnace was heated to 500 °C at a rate of 3 °C min^{-1} and kept at 500 °C for 6 h. After cooling to room temperature, the product was collected and named as HCoPNC.

***Synthesis of Co/CoP-PNCNTs*:** $Co(NO_3)_2 \cdot 6H_2O$ (174 mg), hexamethylenetetramine (70 mg) and trisodium citrate dihydrate (15 mg) were dissolved into the above solution under stirring. Afterword, the mixed solution was heated to 90 ^oC and stirred for 6 h at reflux. After cooling to room temperature, the precipitate ($Co(OH)_2$) was collected by centrifugal separation, washing and vacuum drying. Then, 20 mg of $Co(OH)_2$ and 800 mg of melamine were placed at the downstream and upstream of tube furnace, respectively. Then, the system was heated to 600 ^oC with a heating rate of 5 ^oC min^{-1} under N_2 atmosphere and kept at 600 ^oC for 2 h. After cooling down to room temperature, the product was collected and named as Co-NCNTs. Then 10 mg of Co-NCNTs and 200 mg of NaH_2PO_2 were placed at the downstream and upstream of tube furnace at N_2 flow, respectively. Then, the tube furnace was heated to 500 ^oC at a rate of 3 ^oC min^{-1} and kept at 500 ^oC for 6 h. After cooling to room temperature, the product was collected and named as Co/CoP-PNCTs.

Characterizations

The morphological and structural characteristics of the materials were observed by scanning electron microscopy (SEM, HITACHI SU-8010) and transmission electron microscopy (TEM, FEI Tecnai G2 F20). X-ray diffraction (XRD) analysis was conducted on the X-ray diffractometer (Bruker D8 Advance). Raman spectra was recorded on a micro-Raman spectrometer (LabRAM HR800). X-ray photoelectron spectroscopy (XPS) analysis was performed on the ESCALAB 250Xi. N_2 adsorption/desorption isotherms was collected using Quantachrome Autosorb-IQ2-VP to obtain Brunaure-Emmett-Teller (BET) specific surface area and pore size.

Electrochemical tests

All electrochemical tests were performed on a typical three-electrode system with an electrochemical working station (CHI 700D/660E), where graphitic sheet and Hg/HgO electrode were used as counter electrode and reference electrode, respectively. All mentioned potential has been converted to the relative value *vs.* the reversible hydrogen electrode (RHE) based the following equation:

$$E(vs.RHE) = E^0(Ref) + E(vs.Ref) + 0.059 \times pH \quad \text{(S1)}$$

Working electrode preparation: 5 mg of catalyst and 50 μL of Nafion solution (5%) were dispersed into 600 μL of ethanol solution under ultrasonic treatment to prepare the ink. Then, a certain amount of the ink was dropped onto the surface of rotating disk electrode (RDE) or rotating ring-disk electrode (RRDE). After drying under room temperature, working electrode was obtained with a loading of 400 μg cm^{-2} 。

ORR tests: The catalyst was firstly activated by successive cyclic voltammograms (CVs) in N_2-saturated 0.1 M KOH at a sweep rate of 100 mV s^{-1} between 0 and 1.2 V until steady curves were obtained. Then, stable CVs were recorded at a weep rate of 50 mV s^{-1} in N_2 and O_2 saturated electrolyte, respectively. Meanwhile, linear scan voltammogram (LSV) was obtained at a scan rate of 2 mV s^{-1} from 0 to 1.2 V. The H_2O_2 yield during ORR process was detected by RRDE technique, according to the following equation:

$$\eta_{H_2O_2} = 2 * \frac{I_R/N}{I_D + I_R/N} * 100\% \quad \text{(S2)}$$

Then, the electron transfer number (n) was further determined based the following equation:

$$n = 4 * \frac{I_D}{I_D + I_R/N} \quad \text{(S3)}$$

Where, I_D is the disk current (mA), I_R is the ring current (mA), N is the collection coefficient of ring disk (0.424).

The stability was tested by continuous CVs for 5000 cycles at a rate of 50 mV s^{-1} in O_2-saturated 0.1 M KOH.

OER tests: The catalyst was first activated by continuous CV test at a sweep rate of 50 mV s^{-1} between 1.0 and 1.8 V in O_2-saturated 1.0 M KOH until steady curves were obtained. Then, LSV was conducted at a scan of 2 mV s^{-1} from 1.0 to 1.8 V and then corrected by the resistance compensation (E-i×R_u). Meanwhile, electrochemical impedance spectroscopy (EIS) was conducted in the frequency range from 10^6 Hz to 0.01 Hz with an amplitude of 5 mV at a potential of 1.575 V *vs*. RHE. To evaluate the electrical double layered capacitance (C_{dl}), CV curves were recorded in a non-Faradic region (1.07-1.1.12 V) at different scan rates (20-100 mV s^{-1}). Then, the capacitive current densities of $\Delta j_{|ja\text{-}jc|}$@1.095V/2 were plotted as a function of the CV scan rates. The stability was evaluated via chronopotentiometry test at an oxidized current density of 10 mA cm^{-2} using carbon cloth as the substrate.

Zn-battery tests

The prepared catalyst ink was dropped on the carbon cloth coated with a gas diffusion layer to prepare the air electrode with a catalyst loading of 1.0 mg cm^{-2}. The aqueous Zn-air battery was assembled with the air electrode, Zn-plate anode and the electrolyte. For the primary battery, 6 M KOH solution was used as the electrolyte, while a mixed solution containing 6 M KOH and 0.2 M zinc acetate served as the

electrolyte for rechargeable battery.

The charge and discharge performances were collected on an electrochemical working station (CHI 660E), and the cycling stability was performed using LAND testing system.

DFT calculations

All DFT calculations were carried out using ORCA (version: 5.0.3) [2-4]. Geometry optimization was conducted at the r2SCAN-3c level of theory [5-7]. The single point calculations for the optimized geometries were performed to obtain accurate energies at the ωB97X-V/def2-TZVP level of theory [8, 9]. The solvent effect of water evaluated by the CPCM solvation model [10]. The RIJCOSX approximation was applied with the def2/J auxiliary basis set [11, 12]. The Gibbs free energies were included in the Gibbs energy correction of unscaled vibrational analysis at the r2SCAN-3c level of theory. Electron density difference and density of electronic states were analyzed with MULTIWFN [13, 14], and the results were visualized with VMD software [15].

Results

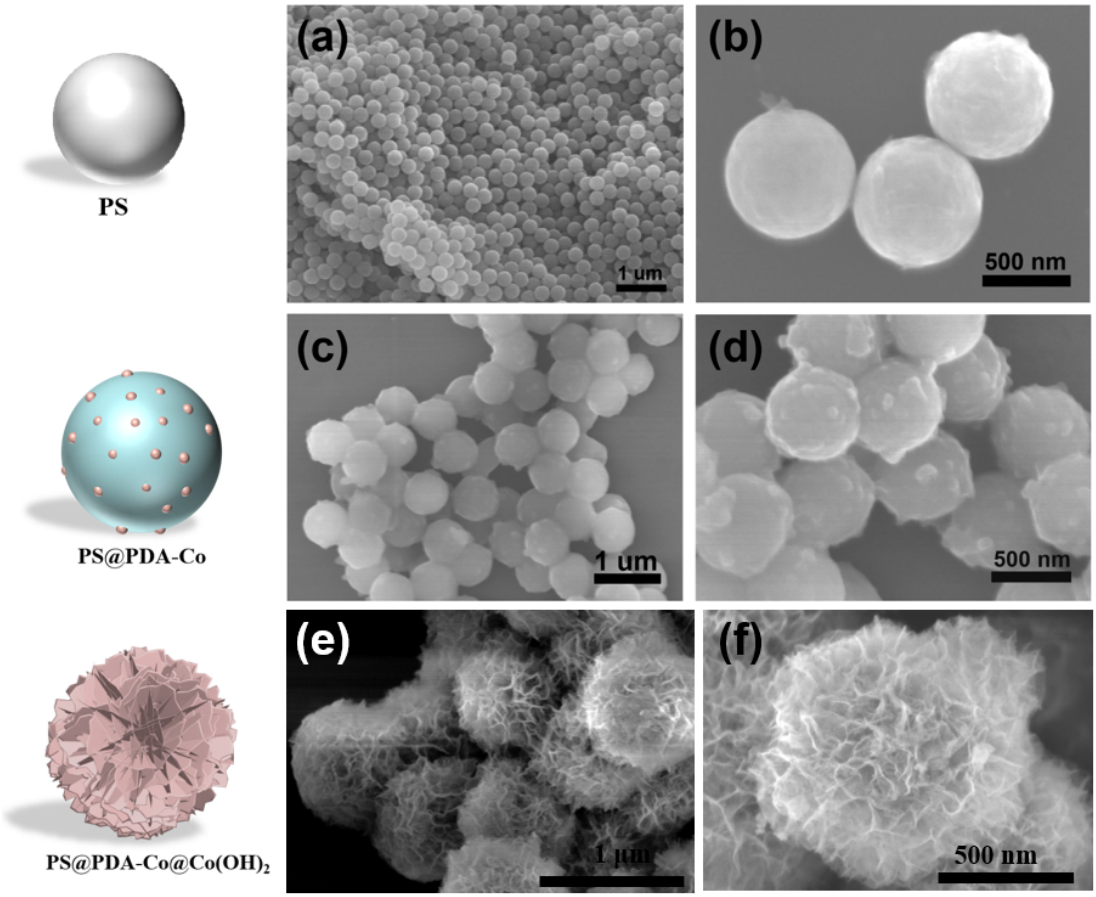

Fig. S1 SEM images of (a, b) PS spheres, (c, d) PS@PDA-Co and (e, f) PS@PDA-Co@$Co(OH)_2$.

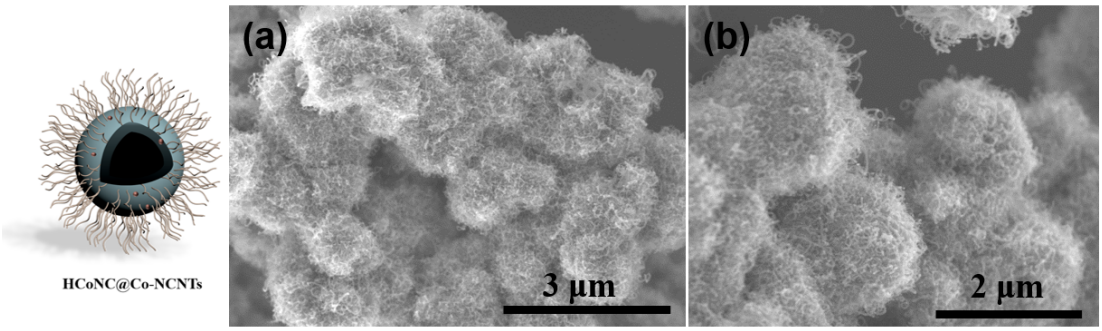

Fig. S2 SEM images of HCoNC@Co-NCNTs.

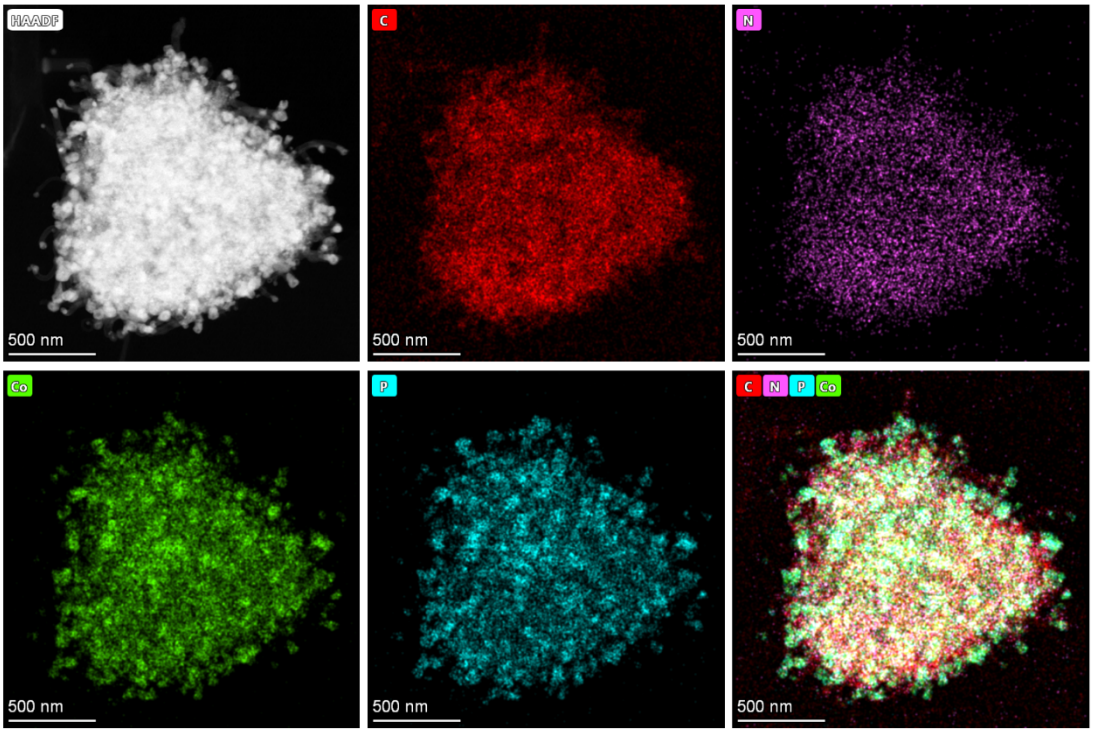

Fig.S3 HADDF-STEM and corresponding EDX elemental mapping images.

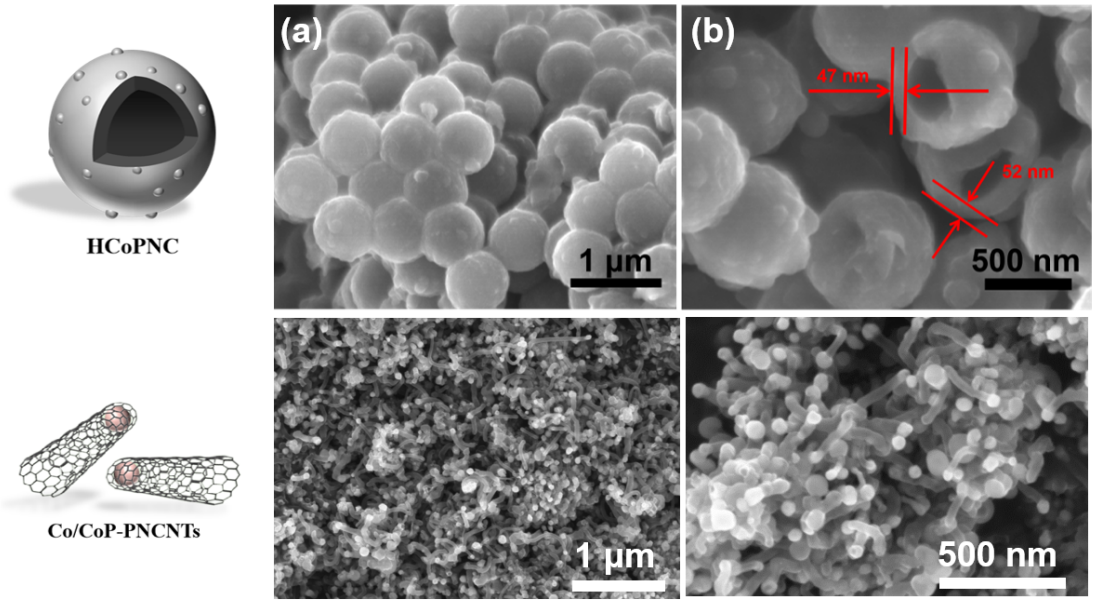

Fig. S4 SEM images of (a, b) HCoPNC, (c, d) Co/CoP-PNCNTs.

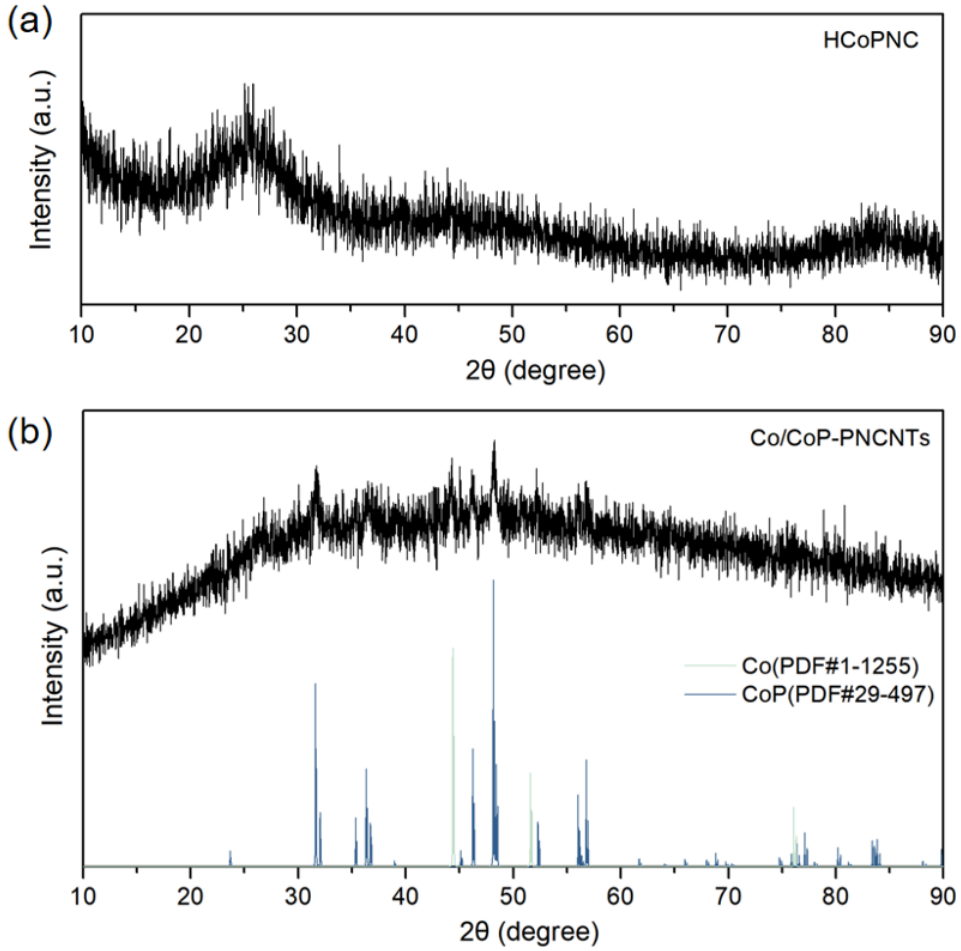

Fig. S5 The XRD patterns of (a) HCoPNC and (b) Co/CoP-PNCNTs.

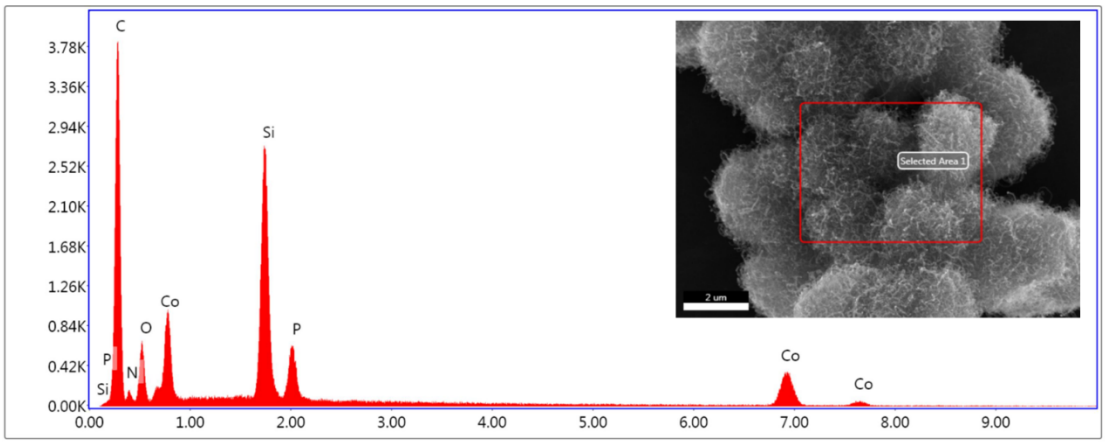

Fig. S6 The EDS of HCoPNC@Co/Co_2P-PNCNTs.

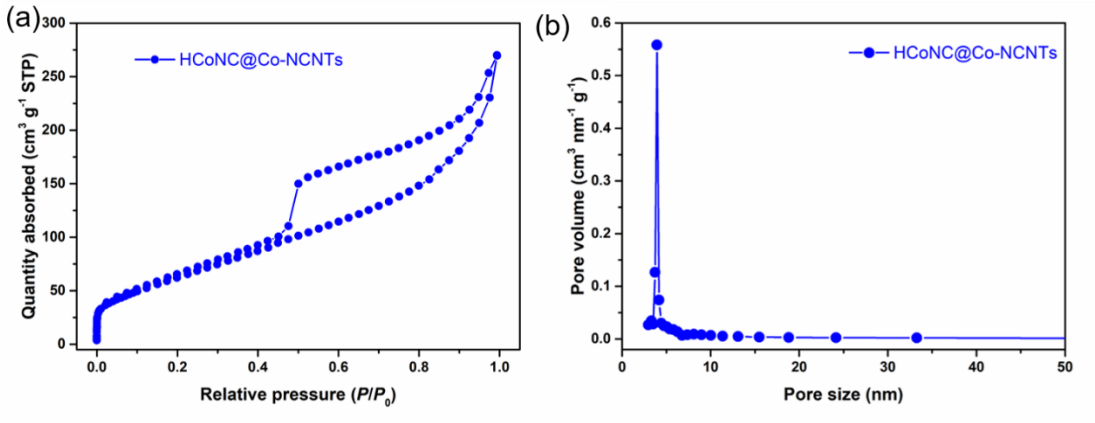

Fig. S7 (a) The N_2 absorption/desorption isothermal and (b) pore-size distribution curve of HCoNC@Co-NCNTs.

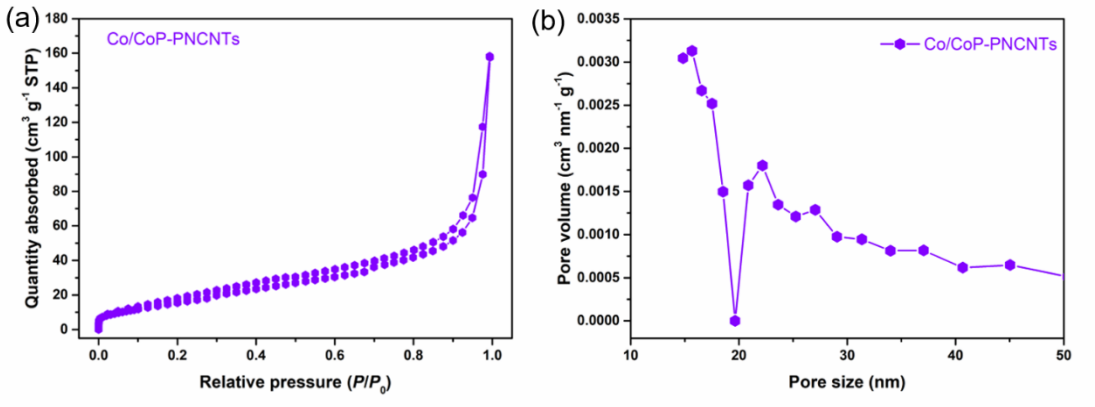

Fig. S8 (a) The N_2 absorption/desorption isothermal and (b) pore-size distribution curve of Co/CoP-PNCNTs.

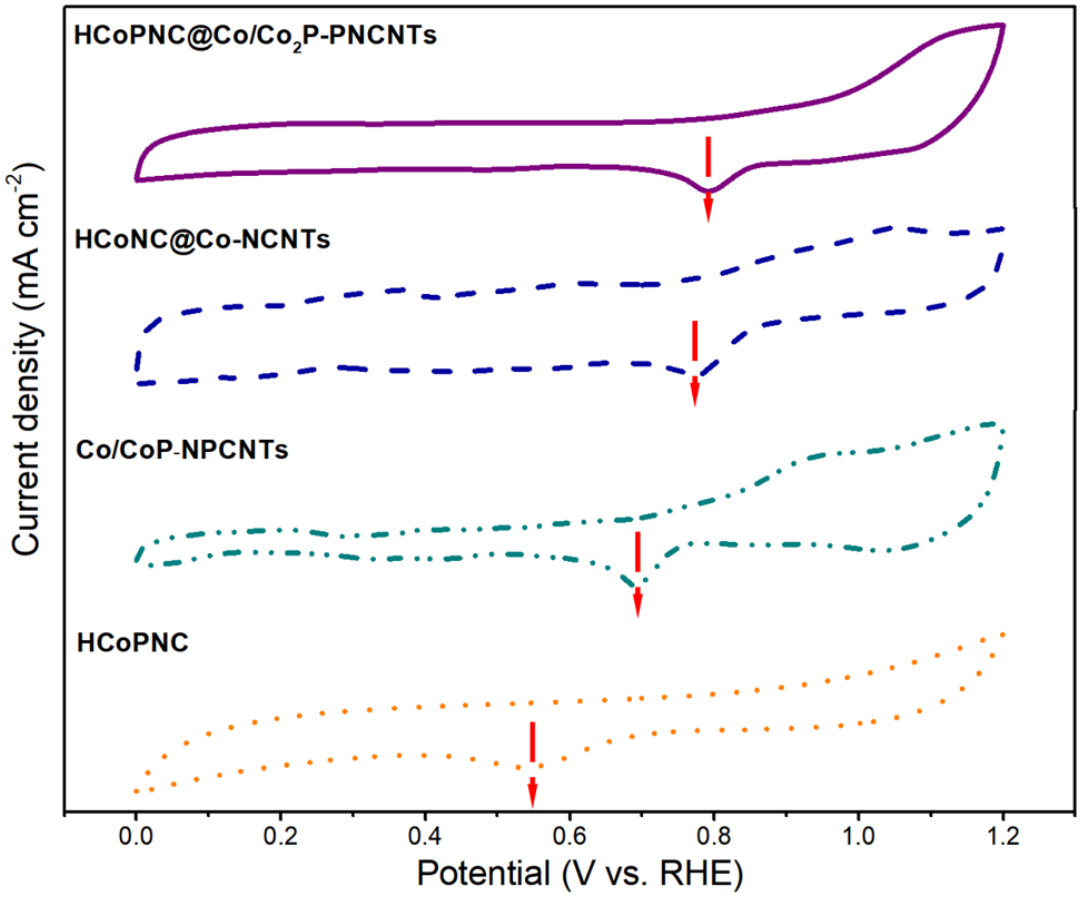

Fig. S9 CV curves of different catalysts in O_2-saturated 0.1 M KOH.

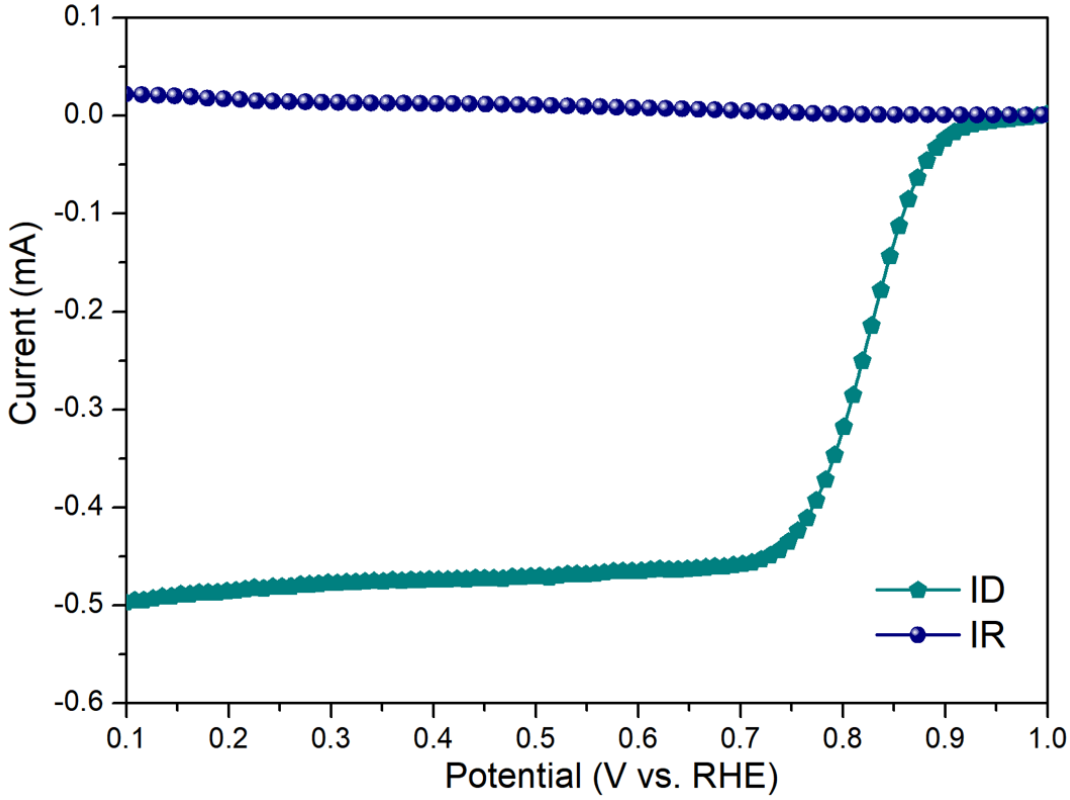

Fig. S10 LSV curves of HCoPNC@Co/Co_2P-PNCNTs measured by RRDE in O_2-saturated 0.1 M KOH.

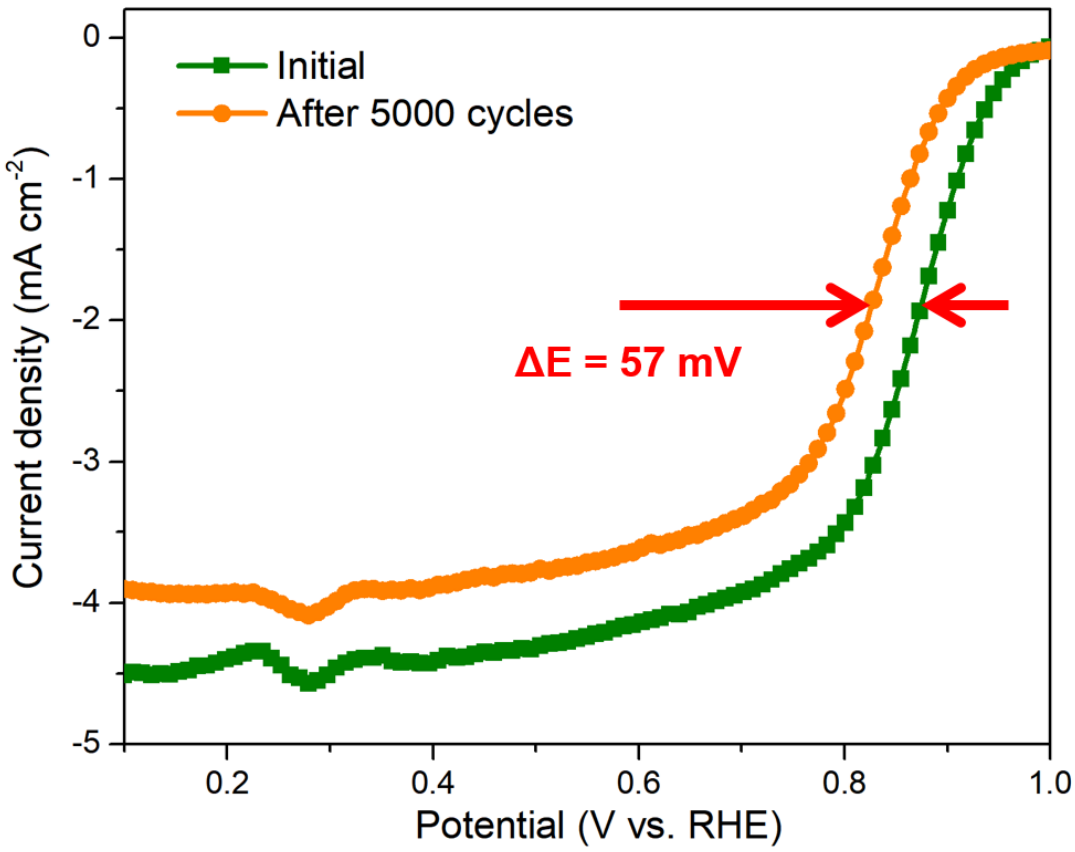

Fig. S11 ORR polarization curves of Pt/C before and after stability test.

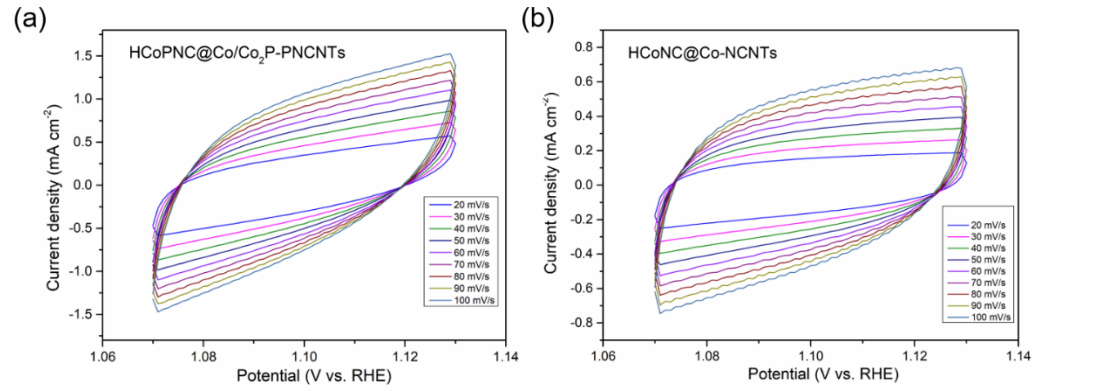

Fig. S12 (a) The CV curves at different scan rates of HCoPNC@Co/Co_2P-PNCNTs;

(b) The CV curves at different scan rates of HCoNC@Co-NCNTs

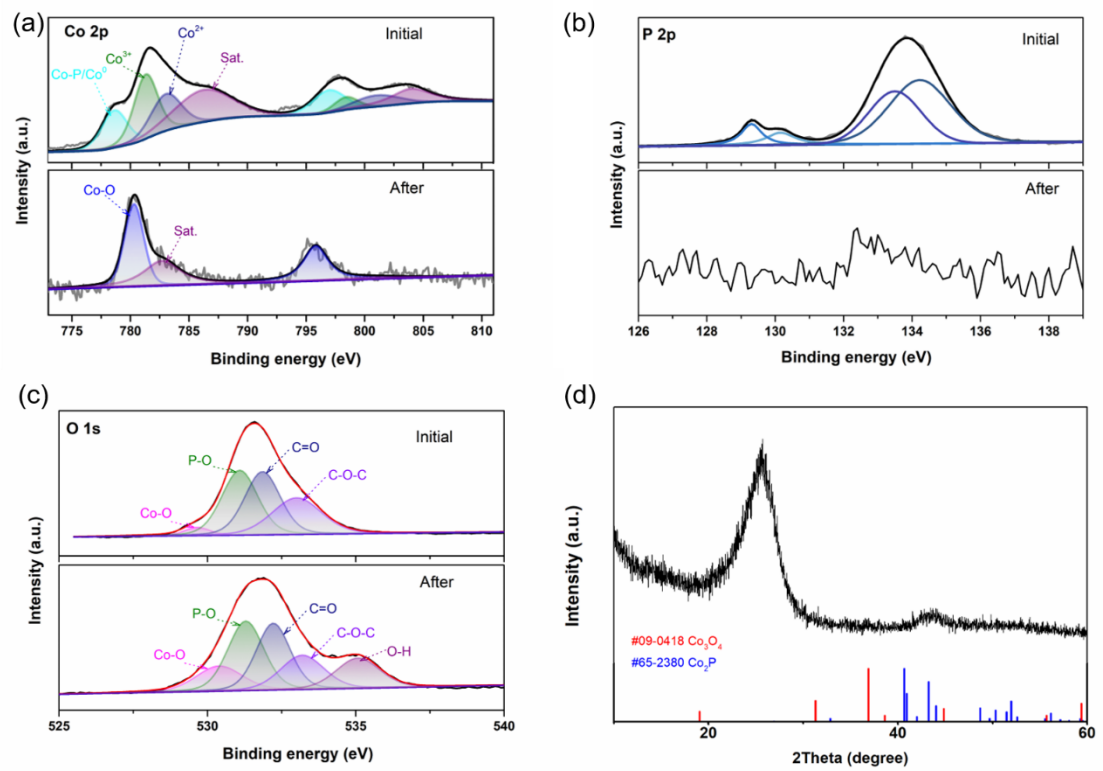

Fig. S13 (a-c) XPS spectra and (d) XRD pattern of HCoPNC@Co/Co_2P-PNCNTs after the OER stability test.

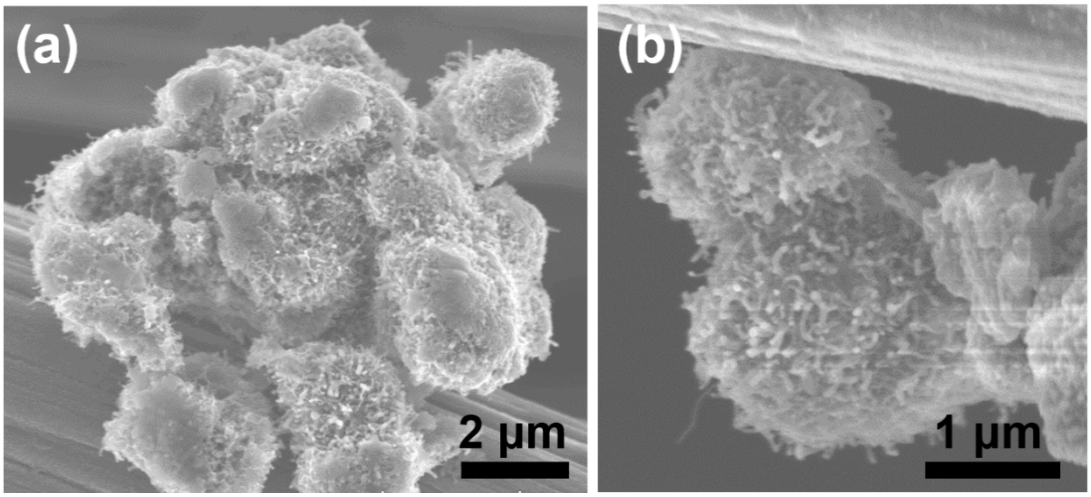

Fig. S14 (a-b) SEM images of HCoPNC@Co/Co_2P-PNCNTs after stability test.

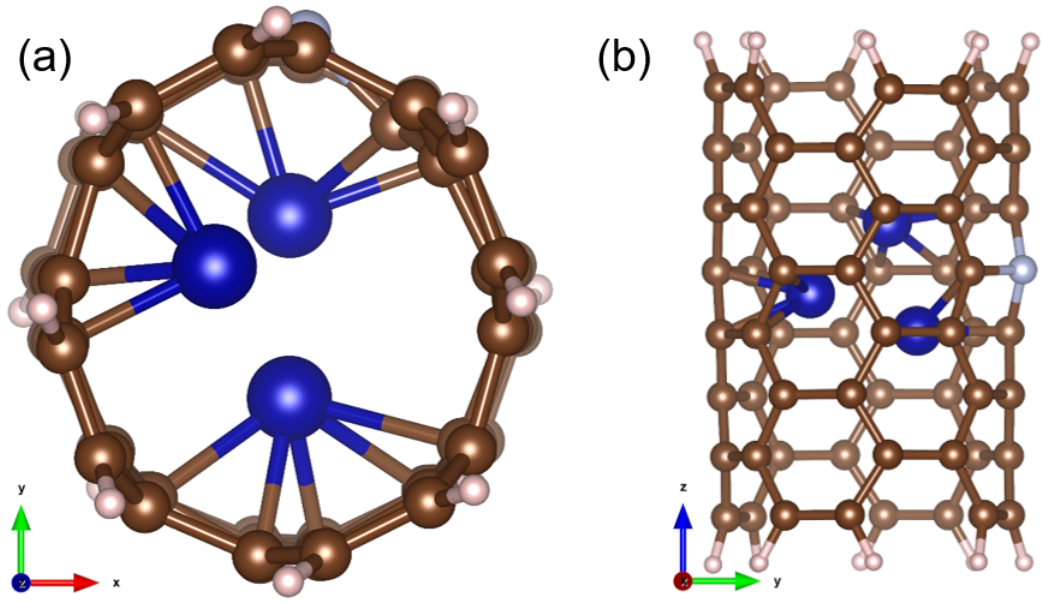

Fig. S15 The optimized geometry of Co@NCNTs.

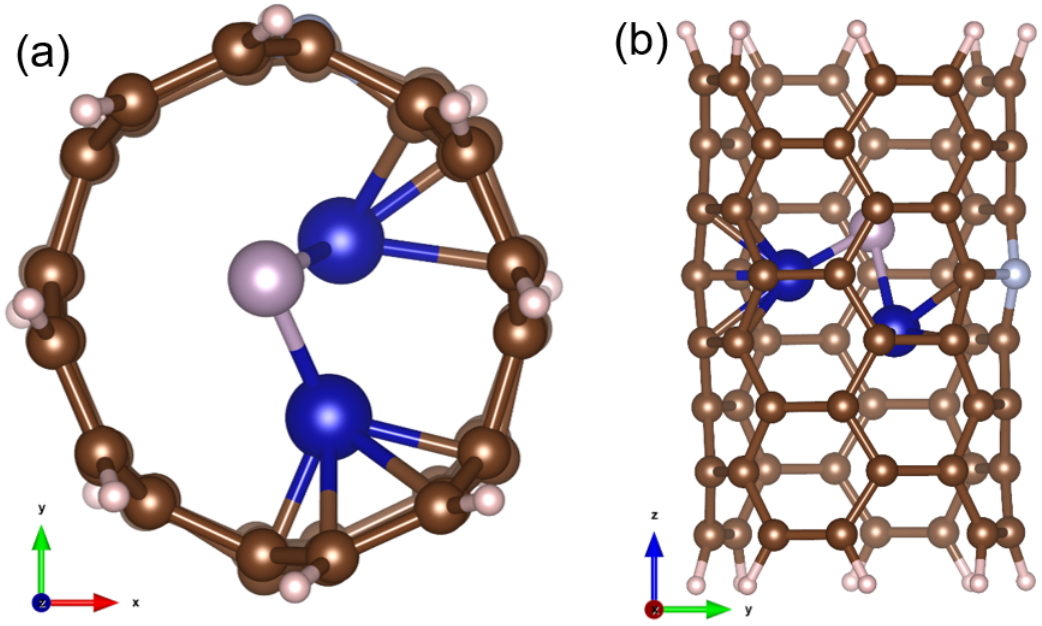

Fig. S16 The optimized geometry of Co_2P@NCNTs.

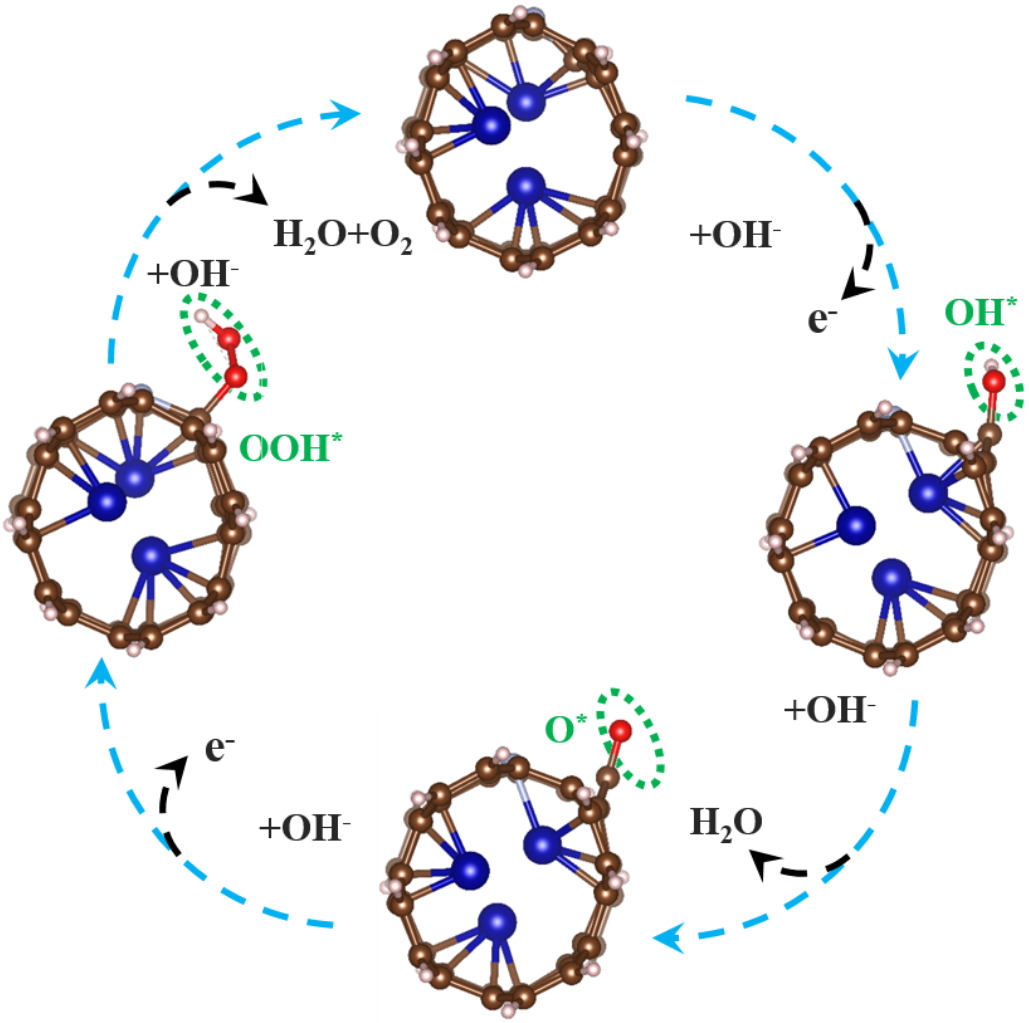

Fig. S17 The optimized geometric configurations of OH*, O* and OOH* in Co@NCNTs.

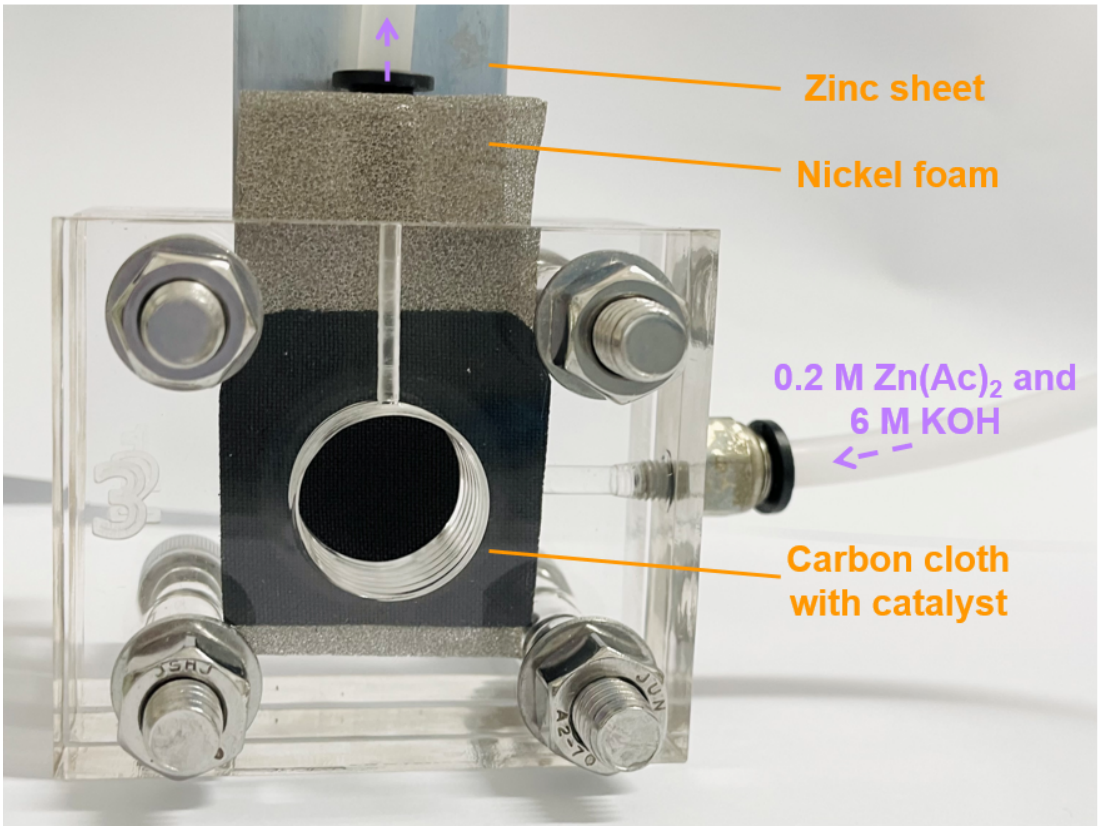

Fig. S18 The digital image of home-made ZAB.

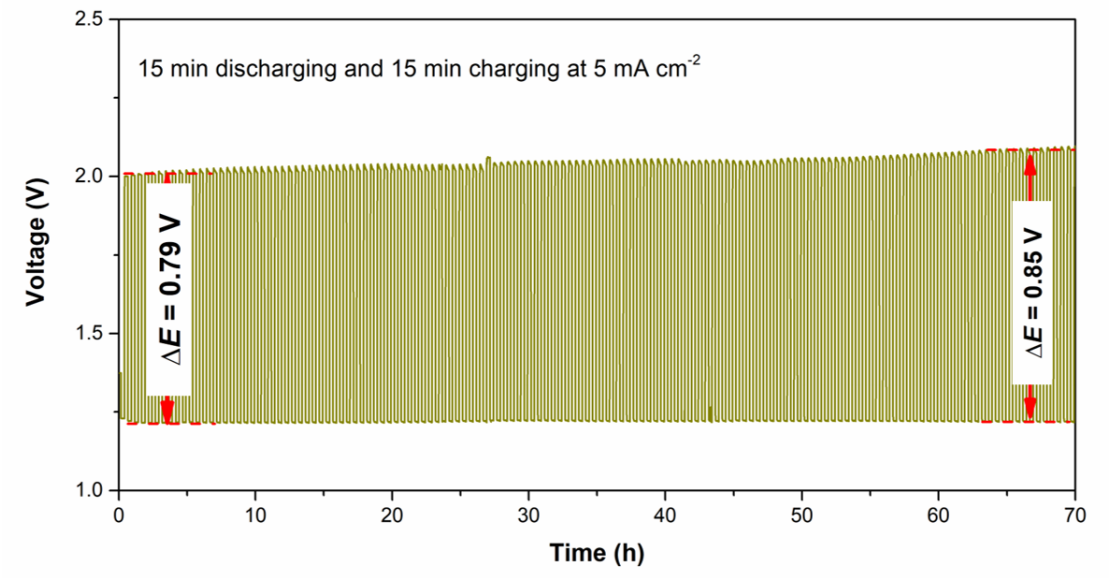

Fig. S19 The discharge/charge cycling stability of HCoPNC@Co/Co_2P-PNCNTs -based ZAB at 5 mA cm^{-2}.

Table S1 Comparison of the ORR, OER and ZAB performances of our catalyst with that in the literature.

Catalysts	$E_{1/2}$ (V vs. RHE) in 0.1 M KOH	$E_{j=10}$ (V vs. RHE) in 1.0 M KOH	Bifunctional activity (ΔE, V)	Peak power density (mW cm^{-2})	Cycling stability	Ref.
HCoPNC@Co/Co_2P-PNCNTs	0.83	1.58	0.75	250	110h@5mA cm^{-2}	This work
Co/Co_2P@NPSC-3	0.86	1.555	0.695	198.1	50h@10mA cm^{-2}	ChemElectroChem, 8 (2021) 4286–4295
Co_2P/CoN-in-NCNTs	0.85	1.65	0.8	194.6	96h@5mA cm^{-2}	Adv. Funct. Mater., 28 (2018) 1805641
Fe-Co_2P/Co@NC	0.876	1.497	0.621	217	155h@10mA cm^{-2}	Chem. Eng. J., 470 (2023) 144380

Co_2P/H-NPC	0.83	1.62	0.79	120	300h@2mA cm^{-2}	J. Energy Storage, 81 (2024) 110440
Co_2P@NPPC	0.85	1.55	0.7	226	160h@10mA cm^{-2}	Catal. Sci. Technol., 13 (2023) 3084–3093
Co_2N/CoP@PNCNTs	0.85	1.559	0.709	151.1	150h@10mA cm^{-2}	Small, 18 (2022) 2108094
Mn(0.1)-Co_2P/NC	0.784	1.6	0.816	40.44	100cycles@10mA cm^{-2}	Mater. Res. Bull., 147 (2022) 111638
Co_2P@NPC	0.82	1.55	0.73	157	140h@10mA cm^{-2}	Energy Environ. Mater., 5 (2022) 515-523
Fe-Co_2P@NPDC	0.895	1.55	0.655	340	83h@1mA cm^{-2}	J. Mater. Chem. A, 10 (2022) 21659–21671

FeCo/FeCoP@NMn-CNS	0.84	1.555	0.715	135	200h@5mA cm^{-2}	J. Colloid Interf. Sci., 605 (2022) 451–462
CoC_x/$(Co_{0.55}Fe_{1.945})_2P$@C	0.84	1.62	0.78	131	60cycles@5mA cm^{-2}	J. Colloid Interf. Sci., 590 (2021) 321–329
Co_2P/CoNPC	0.843	1.556	0.713	116	60h@10mA cm^{-2}	Adv. Mater., (2020) 2003649
CoP–DC	0.81	1.55	0.74	-	-	Adv. Energy Mater., 8 (2018) 1703623
CoP@mNSP-C	0.9	1.64	0.74	-	450h@1mA cm^{-2}	Small, (2017) 1702068
Co/CoP–HNC	0.83	1.53	0.7	-	100cycles@5mA cm^{-2}	Mater. Horiz., 5 (2018) 108-115

Co-Co_2P@NC	0.858	1.598	0.74	120	2000h@2mA cm^{-2}	J. Alloy. Compd., 908 (2022) 164595
FeCoP/NPC	0.855	1.61	0.755	136	1650h@2mA cm^{-2}	Nanoscale, 14 (2022) 12431–12436
CNCP-450	0.78	1.514	0.734	178	50h@10mA cm^{-2}	Energy Technol., (2021) 2100940
CoFeP@C	0.8	1.566	0.766	143.5	200h@2mA cm^{-2}	ACS Appl. Mater. Interfaces, 13 (2021) 22282−22291
CoP NPs/CNSs	0.91	1.57	0.66	-	-	RSC Adv., 9 (2019) 39951–39957
Co-NC@CoP-NC	0.78	1.56 (0.1 M KOH)	0.78	-	-	J. Mater. Chem. A, 4 (2016) 15836–15840

CoP/NP-HPC	0.83	~1.84	1.01	186	80h@2mA cm^{-2}	J. Mater. Chem. A, 8 (2020)19043-19049
Cu_3P/CoP@NC	0.82	-	-	209	317h@5mA cm^{-2}	ACS Nano, 18 (2024) 17901-17912
Zn/CoP	-	1.574	-	93.6	66h@5mA cm^{-2}	Int. J. Electrochem. Sc., 18 (2023) 100153
CoP/Co_2P/Co_3O_4	0.89	1.505	0.615	64.43	33.3h@10mA cm^{-2}	New J. Chem., 46 (2022) 8786-8793

References

[1] H. Lv, S. Wang, Z. Xiao, C. Qin, S. Zhai, G. Wang, Z. Zhao, Q. An, J. Power Sources, 2021, 493, 229679.

[2] F. Neese, Wiley Interdiscip. Rev.: Comput. Mol. Sci. 2012, 2,73–78.

[3] F. Neese, Wiley Interdiscip. Rev.: Comput. Mol. Sci. 2018, 8, e1327.

[4] F. Neese, Wiley Interdiscip. Rev.: Comput. Mol. Sci. 2022, 12, e1606.

[5] S. Grimme, A. Hansen, S. Ehlert, J.-M. Mewes, J. Chem. Phys. 2021, 154, 064103.

[6] M. Gawron, F. Gilch, D. Schmidhuber, J. A. Kelly, T. M. Horsley Downie, A. J. Wangelin, J. Rehbein, Robert Wolf, Angew. Chem. 2024, 63, e202315381.

[7] J. Malenfant, L. Kuster, Y. Gagné, K. Signo, M. Denis, S. Canesi, M. Frenette, Chem. Sci., 2024, 15, 701-709.

[8] N. Mardirossian, M. Head-Gordon, Phys. Chem. Chem. Phys., 2014,16, 9904-9924.

[9] N. Mardirossian, M. J. Head-Gordon, Chem. Phys., 2016, 144, 214110.

[10] A. V. Marenich, C. J. Cramer, D. G. Truhlar, J. Phys. Chem. B, 2009, 113, 6378-6396.

[11] F. Neese, F. Wennmohs, A. Hansen, U. Becker, J. Chem. Phys., 2009, 356, 98-109.

[12] F. Weigend, Phys. Chem. Chem. Phys., 2006, 8, 1057-1065.

[13] T. Lu, F. W. Chen, J. Comput. Chem., 2012, 33, 580-592.

[14] T. Lu, J. Chem. Phys., 2024, 161, 082503.

[15] W. Humphrey, A. Dalke, K. Schulten, J. Mol. Graph., 1996, 14, 33-38.